TUDelft

Delft University of Technology

4×2 Hot electron bolometer mixer arrays for detection at 1.4, 1.9, and 4.7 THz for the balloon-borne terahertz observatory GUSTO

Gaspar Silva, Jose Rui; Laauwen, Wouter; Mirzaei, B.; Vercruyssen, N.; Finkel, M.; Westerveld, M.; Young, Abram; Kulesa, Craig; Gao, J.R.; More Authors

RESEARCH PAPER

4 × 2 Hot electron bolometer mixer arrays for detection at 1.4, 1.9, and 4.7 THz for the balloon-borne terahertz observatory GUSTO

Jose Rui G. Silva [a,b,*] Wouter M. Laauwen,[a] Behnam Mirzaei,[a,c] Nathan Vercruyssen,[a,c] Matvey Finkel,[a] Menno Westerveld,[a] Nikhil More,[a] Vitor Silva,[a] Abram Young,[d] Craig Kulesa,[d] Christopher Walker,[d] Floris van der Tak,[a,b] and Jian Rong Gao [a,c,*]

[a]SRON Netherlands Institute for Space Research, Groningen and Leiden, The Netherlands
[b]University of Groningen, Kapteyn Astronomical Institute, Groningen, The Netherlands
[c]Delft University of Technology, Optics Research Group, Department of Imaging Physics, Delft, The Netherlands
[d]University of Arizona, Steward Observatory, Tucson, Arizona, United States

ABSTRACT. We have successfully demonstrated three 4 × 2 hot electron bolometer (HEB) mixer arrays, designed to operate between 4.2 and 5.5 K, with local oscillator (LO) frequencies of 1.4, 1.9, and 4.7 THz, respectively. These arrays consist of spiral antenna coupled NbN HEB mixers combined with elliptical lenses. These are to date the highest pixel count arrays using a quasi-optical coupling scheme at supra-THz frequencies. At 1.4 THz, we obtained an average double sideband mixer noise temperature of 330 K, a mixer conversion loss of 5.2 dB, and an optimum LO power of 210 nW. The array at 1.9 THz has an average mixer noise temperature of 425 K, a mixer conversion loss of 6.4 dB, and an optimum LO power of 190 nW. For the array at 4.7 THz, we obtained an average mixer noise temperature of 715 K, a mixer conversion loss of 8.9 dB, and an optimum LO power of 240 nW. We found the arrays to be uniform regarding the mixer noise temperature with a standard deviation of 3% to 4%, the conversion loss with a standard deviation of 8% to 11%, and optimum LO power with a standard deviation of 5% to 6%. The noise bandwidth was also measured, being 3.5 GHz for the three arrays. These performances are comparable to previously reported values in the literature for single pixels and also other detector arrays at similar frequencies. Our arrays met the instrument requirements and were employed in the Galactic/Extra-Galactic ULDB Spectroscopic Terahertz Observatory (GUSTO), a NASA balloon-borne observatory. GUSTO launched from Antarctica on the 31st of December 2023 having a successful flight of 57 days, the longest ever recorded by NASA for such a mission profile.

© 2025 Society of Photo-Optical Instrumentation Engineers (SPIE) [DOI: 10.1117/1.JATIS.11.1.016001]

Keywords: GUSTO; hot electron bolometer; lens-antenna; mixer array

1 Introduction

The supra-terahertz (THz) frequency range between 1 and 6 THz is very interesting and important for astronomy because it is rich in diagnostic atomic fine-structure lines (e.g., [CII], [NII], [OI]), high-J lines of heavy molecules (e.g., CO) and ground-state lines of hydrides (e.g., H_2O, HD).[1] With the use of high-resolution spectroscopic techniques based on a heterodyne receiver,

---

*Address all correspondence to Jose Rui G. Silva, j.r.g.d.silva@sron.nl; Jian Rong Gao, j.r.gao@sron.nl

it is possible to measure not only the line intensity but also to resolve the frequency line profile, which allows one to extract information regarding the velocities of interstellar gas clouds. With such detailed information, one can unveil the dynamics and processes that dominate, for example, in regions of star and planet formation.[2–5] Another application of heterodyne receivers at terahertz frequencies is interferometry, which enables to spatially resolve objects with a high angular resolution of sub-arcsec.[6]

The core of a heterodyne receiver is a mixing element, where the sky signal is mixed with a strong and well-known signal from a local oscillator (LO). During the mixing, the sky signal is down-converted to the frequency difference between the sky and LO signals, named intermediate frequency (IF). This IF signal is in the GHz range, which makes it easier to be amplified and processed by common electronics. Furthermore, a sufficiently large IF bandwidth is needed for the detection of at least an entire spectral line without the need to tune the LO frequency. At THz frequencies, the best-performing mixer devices are the superconductor-isolator-superconductor (SIS) junctions[7,8] and the hot electron bolometers (HEBs).[9,10] SIS mixers are based on photon-assisted tunneling in the junction, having the highest sensitivity and largest IF bandwidth among the two types of mixers.[11] Because of this, for frequencies up to 1 THz SIS mixers are the detector of choice for heterodyne instruments, such as those for the Atacama large millimeter/submillimeter array.[12] However, above ~1.2 THz, the performance of SIS mixers degrades rapidly due to the finite energy gap of the superconducting material used, combined with increased losses in the on-chip inductive tuning circuit. This circuit is required to compensate for the junction capacitance. HEBs are based on the bolometric effect, where a change in temperature induces a change in resistance. They do not suffer from the upper-frequency limitation, in contrast to SIS, which makes them the mixer of choice for the heterodyne instruments that operate above 1 THz. The best-performing HEBs are so far based on the superconducting niobium nitride (NbN)[10] and have been demonstrated up to 5.3 THz.[13] NbN HEBs on Si substrates, with reasonable receiver noise temperatures have shown a typical IF bandwidth of 3 to 4 GHz.[14,15] Such devices have been previously used in instruments such as HIFI on the Herschel Space Observatory,[15,16] the STO-2 balloon-borne observatory[17] and upGREAT on the SOFIA air-borne observatory.[18] Different types of coherent sources have been employed as LOs depending on the target frequency. For frequencies below ~2 THz the preferred LOs are solid-state sources based on frequency multiplier-chains[19,20] because they can be operated at room temperature and have a sufficiently wide frequency tuning range of ≥15%.[20] Starting from ~2 THz, quantum cascade lasers (QCLs)[21,22] dominate because they can be operated at any frequency within the range between 1.3 and 5 THz with sufficient output power. The frequency for the QCLs that were used or are suitable as LO can be tuned electrically by varying the bias voltage. However, the tuning range is so far limited to ≤10 GHz,[23] which is only a small fraction of the operating frequency. With novel approaches, e.g., a QCL by applying a metasurface in combination with vertical-external cavity surface-emitting-laser structure, a 20% fractional tuning is possible.[24] Furthermore, THz QCLs are typically operated at temperatures between 40 and 70 K, which can be provided by Stirling coolers.

With recent advancements in mixer technology, the sensitivity of NbN HEBs has significantly been improved, approaching levels that are only a few times the quantum limit (hf/2 k) defined for the single sideband (SSB). For instance, at 1.6 THz, our group has demonstrated a considerable improvement in DSB mixer noise temperature, achieving a reduction of ~30% relative to previous reports,[25] with values as low as 6.2× hf/2 k. In addition, another study[13] has reported achieving DSB mixer noise temperatures as low as 4.2× hf/2 k at 5.3 THz. Further improvements to a DSB receiver noise temperature, if possible, have a limited room with maximally a factor of ~2 at the high end of the supra-THz frequency range, as suggested in Ref. 13. On the other hand, some of the sources or structures of astronomical interest, e.g., giant molecular clouds, span angular scales much larger than the field of view of a telescope, which need to be scanned or mapped. A single-pixel receiver placed at the focal point of the telescope is relatively inefficient as it samples only a small part of the field of view of the telescope. In this case, a multi-pixel detector array positioned at the focal plane of a telescope can therefore increase the efficiency of the observatory,[26] where the mapping speed of the instrument scales roughly with the number of pixels in the array.[27,28] However, only recent advances in some critical technologies have made receiver systems using multi-pixel arrays possible for airborne,[18] balloon-borne,[29–31]

and proposed instrument concepts for future space THz observatories.[32–34] The critical technologies include frequency multiplier-chain-based multi-beam LOs,[35] high power QCLs,[23,36] and LO multiplexing schemes based on Fourier phase gratings.[37,38]

Until recently, only STO-2[17] and upGREAT[18] instruments have utilized detector arrays at supra-THz frequencies. STO-2 employed 2-pixel arrays at 1.4 and 1.9 THz, consisting of quasi-optically coupled HEB mixers, namely using a lens-antenna scheme. upGREAT used to operate a 14-pixel array at 1.9 THz, which consisted in the practice of two 7-pixel arrays for detecting two orthogonal polarizations. Besides, upGREAT used also a 7-pixel array at 4.7 THz. The upGREAT mixer arrays were based on feedhorn-waveguide structures to couple the radiation from free space to the HEB and were comprised of multiple individual mixers on physically separated blocks. In other words, they are not built on a monolithic block. Such mixers have the advantage of being easier to align and match with the instrument optics; however, they occupy a relatively large volume in the instrument, which is in contrast to the need for space instruments, where small and compact arrays are preferred. Furthermore, with this approach, it is hard to realize a much larger array, e.g., 64 pixels. Recent work shows potential for monolithic waveguide blocks,[38] but no such mixer array has been demonstrated yet.

GUSTO[29,30] was a NASA balloon-borne THz observatory that aimed at exploring the inner dynamics of the Milky Way and the Large Magellanic Cloud using three heterodyne array receivers to map the fine structure lines of [NII] at 1.46 THz, referred to as Band 1 (B1), [CII] at 1.9 THz (B2) and [OI] at 4.7 THz (B3). GUSTO was launched from the Long Duration Ballon facility in Antarctica on the 31st of December 2023 with a successful flight of 57 days, the longest ever recorded for this type of mission. GUSTO used compact 4 × 2 HEB mixer arrays. As LOs, for B1 and B2, it used frequency multiplier chain arrays developed by Virginia Diodes Inc., Charlottesville in the United States.[35] For the B3 receiver, it employed a multi-beam LO in a 4 × 2 pattern generated using a QCL developed by MIT at Cambridge in the United States,[23] which was multiplexed by an asymmetric Fourier phase grating developed by SRON/TUDelft.[38]

The focus of this paper is the experimental characterization of the three 4 × 2 HEB mixer arrays (with 24 pixels in total) developed for the GUSTO receivers. Due to technical issues and mission deadlines, not all pixels were used during the final flight. Therefore, we believe that it is better to describe the array performance during GUSTO's integration and flight in a separate paper.

We focus our characterization on the DSB mixer noise temperature ($T_{\text{mixer}}^{\text{DSB}}$), the mixer conversion loss ($L_{\text{mixer}}^{\text{DSB}}$) and the optimum LO power requirement (P_{LO}) at the mixer array level. These parameters represent the figures of merit used in the requirements set for the HEB mixers needed for GUSTO. The goal in the development of these arrays was to meet the instrument performance requirements. These arrays use a quasi-optical coupling scheme based on an elliptical lens combined with a logarithmic spiral antenna, making them the largest quasi-optical mixer arrays in the supra-THz region so far. The architecture used in our arrays can be scaled to a high pixel count (>64 pixels), as discussed at the end of the paper.

Our paper is organized as follows. In Sec. 2, we start by introducing the instrument requirements and the different array architectures and then describe the assembled detector arrays. In Sec. 3, we highlight the experimental setup used to characterize the arrays. Section 4 presents the characterization results of the arrays. The paper ends with the conclusions.

2 HEB Mixer Arrays

In Table 1, we summarize the performance requirements of the HEB mixer arrays for GUSTO regarding sensitivity, LO power, and IF bandwidth. GUSTO scientific goals required an average SSB system noise temperature ($T_{\text{sys}}^{\text{SSB}}$) of 2900 K at 1.46, 2700 K at 1.9 THz, and 3000 K at 4.7 THz. These requirements can be broken down into allocations at the mixer array level in the form of a pair, $T_{\text{mixer}}^{\text{DSB}}$ and $L_{\text{mixer}}^{\text{DSB}}$, for each array, shown in Table 1. Here, we define $T_{\text{mixer}}^{\text{DSB}}$ as the noise temperature after removing the contribution caused by the optical losses in front of the lens and the noise contribution from the IF chain. This value is defined at an IF frequency of 2 GHz. Instead of using the typical receiver noise temperature and conversion gain, we focus on the parameters of $T_{\text{mixer}}^{\text{DSB}}$ and $L_{\text{mixer}}^{\text{DSB}}$ because our experimental setup for characterizing the mixer arrays differs from the actual flight receiver system. The optics and IF chains

Table 1 GUSTO RF and IF requirements for each pixel in the HEB mixer arrays.

Lens type	Operating frequency (THz)	T_{mixer}^{DSB} (K)	L_{mixer}^{DSB} (dB)	P_{LO} (nW)	IF bandwidth (GHz)
B1	1.46	650	10.5	155 to 270	3
B2	1.9	650	10.5	155 to 270	3
B3	4.7	700	11	155 to 270	4

T_{mixer}^{DSB} and L_{mixer}^{DSB} are the pixel noise temperature and conversion loss, respectively, defined in front of the lens, see main text. T_{mixer}^{DSB} is defined at an IF frequency of 2 GHz. P_{LO} is the mixer optimum LO power at the HEB.

in our lab setup are not the same as those used in the final instrument. Therefore, focusing on receiver performance in the lab would not accurately reflect the instrument's expected performance. By quantifying and discussing both T_{mixer}^{DSB} and L_{mixer}^{DSB}, we isolate the intrinsic performance of the mixer array, independent of the test setup optics and IF chain. In summary, these figures provide a more accurate basis for comparing the performance of the same mixers across different systems. The LO power requirement, P_{LO}, is determined by the available LO power from the sources, the tuning range, and the optical losses between these sources and HEB mixers. In the cases of B1 and B2, the higher end of the requirement (270 nW) was estimated to require ≈3 to 4 μW for each LO source per pixel. This power was enough to account for all-optical losses and a 13-μm mylar beam splitter (with a reflectivity of 12% at 1.46 and 1.9 THz). For B3, the LO was designed to utilize a single QCL beam with a power output exceeding 1.6 mW. This configuration considered the QCL beam's 10% gaussicity, employed a 1-to-8 beam multiplexing with a 70% efficiency,[38] and used a similar beam splitter configuration as in B1 and B2. The IF bandwidth is defined as the frequency point where the receiver noise temperature increases by 3 dB. This requirement represents the IF frequency range required to cover the necessary range of velocities, and Doppler shifts of the emission lines, enabling instantaneous observations of the target scientific objects, assuming all other requirements are nominally met.

All HEB mixer arrays were designed to allow for eight pixels in a 4 × 2 configuration within a single metal block. All the pixels in an array share the same basic configuration that is shown in Fig. 1(a). For each pixel, THz radiation is collected on the surface of the elliptical Si lens.
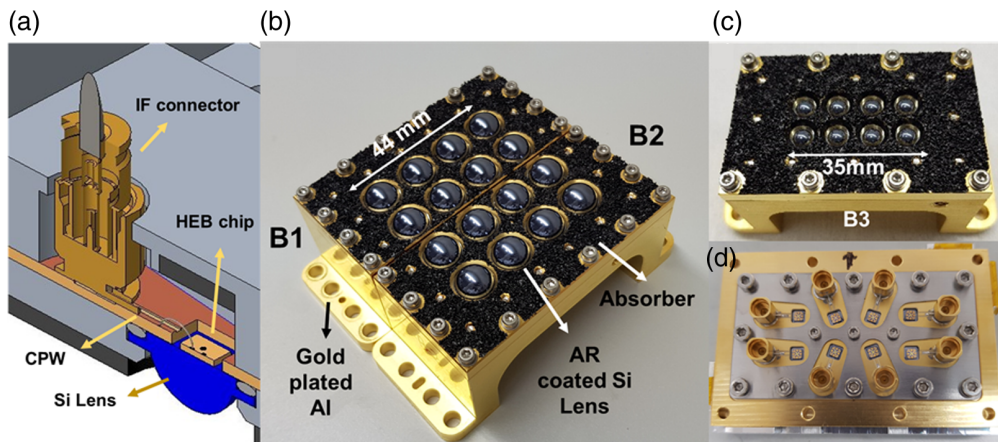
Fig. 1 4 × 2 HEB mixer arrays. (a) Schematic of the single pixel configuration used in all the arrays. THz radiation is collected at the elliptical surface of the lens and focused on the HEB antenna. The HEB is connected through bonding wires to a CPW transmission line, which is used to both bias the device and carry out the IF signal from the mixer. The other end of the CPW line is terminated with an IF connector that is the interface to an LNA. (b) Completed B1 and B2 arrays, for operation at 1.46 and 1.9 THz, respectively. The arrays are presented side by side, mimicking a 4 × 4 array. This is the actual placement on the cold plate of the GUSTO instrument. (c) Completed B3 array designed to operate at 4.7 THz. (d) A backside view of the partly assembled B3 array, where the eight HEB chips, CPW lines, and IF connectors are shown, from Ref. 39.

It is then focused, as it propagates through the lens and HEB chip substrate, to the spiral antenna, where the radiation is converted to an AC electrical current that is fed to the HEB. Through bonding wires, the HEB is connected to a co-planar waveguide (CPW) line that is used to both DC bias the device and collect the IF signal from the mixer. Each pixel is terminated with an IF connector that acts as the interface to a low noise amplifier (LNA). In the array, the IF lines are placed such that no IF cross-talk is present in the assembled circuit board. To confirm this, we measured an $S_{21} < -60$ dB, where S_{21} represents the power transferred from port 1 to port 2, with each port in our case being a different IF line.

The lenses and the substrate of the HEB chips are made of pure, highly resistive Si (≥ 5 k$\Omega \cdot$ cm), which has a negligible optical loss at cryogenic temperatures.[40] Each HEB chip consists of an NbN bridge integrated with a planar logarithmic spiral antenna. We chose such an antenna because it has a high power coupling efficiency to the HEB bridge over a wide range from 1 to 5.3 THz.[13,41,42] Other options, such as twin slot antennas, have never been demonstrated for low-noise HEB mixers above 2.5 THz.[43] In addition, because of the wide-band coverage of a spiral antenna, we can apply a common design for the arrays operated at the three different frequencies, which reduces the cost significantly. The antenna structure is similar to the one used in Ref. 41. The logarithmic spiral antenna used 3 has a starting radius $k = 4$ μm, curvature $a = 0.318$ and arm width $\delta = 83$ deg. Elliptical lenses were chosen since they offer high coupling of the radiation to an antenna and also higher gaussicity of the beam compared to a hemispherical lens.[44]

Two models of detector arrays were designed to accommodate the two types of lenses with different diameters. In Fig. 1(b), we show the completed B1 and B2 arrays, using 10-mm diameter lenses and having a pitch size of 11 mm. The two arrays make use of the same model and were optimized for operation at 1.46 and 1.9 THz, respectively. Because these two frequencies are very close, it is difficult to separate them in the optical path of the instrument. Thus, B1 and B2 were designed to be placed side by side on the cold plate of the cryostat, mimicking a 4 × 4 array. The devices used have an NbN bridge of 2 μm in width, 0.15 μm in length, and 5 nm in thickness. Besides a good impedance matching between the HEBs and the antennas, such dimensions of the HEBs provide an optimum LO power within the requirements described in Table 1. The critical temperature of the NbN bridges is about 10 K. In Fig. 1(c), we show the completed B3 array that uses 5-mm diameter lenses and has an 8-mm pitch size. This array is optimized for operation at 4.7 THz. In Fig. 1(d), we present a back-side view of the B3 array, while partly assembled, where the eight detector chips, CPW lines, and IF connectors are shown. The HEB devices used in this array are similar to the ones used in the other arrays (from the same wafer); however, the NbN bridge lengths are longer, being 0.2 μm instead. The increased HEB length increases the volume of the HEB, and thus, the LO power required.

Each of the arrays has a different lens design, optimized to meet the GUSTO optical beam requirements. The optimization study and verification can be found in Ref. 45. The detailed lens designs are shown in Table 2. In addition, each lens is coated with Parylene C as an anti-reflection (AR) coating with the ideal thickness, designed using Eq. (2) in Ref. 46. Both realized (measured) and designed thicknesses of the Parylene C are also shown in Table 2. The differences are due to the limited accuracy in controlling the thickness during the coating process. The

Table 2 Characteristic parameters of the lenses and AR coating for three different frequencies.

Lens type	Operating frequency (THz)	Major axis (μm) ±2 μm	Minor axis (μm) ±2 μm	Extension length (μm) ±2 μm	Parylene-C thickness (μm) ±0.2 μm
B1	1.46	5235	5000	1542	33 (31.7)
B2	1.9	5235	5000	1527	24.5 (24.4)
B3	4.7	2617	2500	767	1.1 (9.8)

Each lens type is used in a different array. The extension length includes the detector substrate, which has a thickness of 342 ± 2 μm. For the Parylene-C, we present first the realized thickness and in parentheses the ideal, designed thickness.

methodology used to mount and align the HEB antenna with the lens optical axis has been described elsewhere.[39]

3 Experimental Setup

We measure the DSB receiver noise temperature ($T_{\mathrm{rec}}^{\mathrm{DSB}}$), the receiver conversion loss ($L_{\mathrm{rec}}^{\mathrm{DSB}}$), and the required LO power (P_{LO}) for each pixel in the arrays. The measurements for the three arrays were performed at 1.39, 1.63, and 5.25 THz, respectively, being slightly different from GUSTO's respective B1, B2, and B3 center frequencies. Because we do not have the same LOs as GUSTO available at SRON (where the experiments were performed), the choice of characterization frequency for the different mixer arrays was limited to the closest THz lines available from the far infrared (FIR) gas laser used as LO in our heterodyne measurement setup. The IF noise bandwidth (NBW) was measured in the IF frequency range between 0.5 and 5 GHz for a few selected mixers. In addition, the beam properties and pointing direction of the mixers were also characterized and can be found elsewhere.[39,45]

The heterodyne measurement setup used in our experiments is schematically presented in Fig. 2. The LO is a FIR gas laser operated at 1.39, 1.63, or 5.25 THz. We use a swing arm optical attenuator[47] in combination with a proportional-integral-derivative feedback loop to sweep or stabilize the LO power when measuring $T_{\mathrm{rec}}^{\mathrm{DSB}}$.[48] This methodology allows for sweeping the current of a HEB at a given voltage for both the hot and cold load measurements, thereby determining the Y-factor at the exact same DC bias point without being influenced by fluctuations and drift in the FIR laser power. Using this approach, the same current is achieved by making a small adjustment in LO power to compensate for the power difference coupled to the detector between the hot and cold load. Conceptually, because the LO power is different, the mixer gain also changes. However, measurements with a similar device, where we added an optical narrow bandpass filter, showed that after correcting for the optics, we obtained very similar noise temperatures in both cases. This indicates that our methodology is valid. The reason is that the LO power change is very small, on the order of 2% to 4%, causing a negligible change in mixer gain. This observation aligns with previous studies from our group.[49,50]

The radiation from both the LO and the blackbody load, being either hot (at a temperature of 290 to 295 K) or cold (77 K), are combined with a 3-μm thick Mylar beam splitter. The combined radiation propagates through a 1.2-mm thick ultra-high molecular weight polyethylene cryostat window and a QMC heat filter with a cut-off frequency of 5.8 THz at 4 K, to the lens of the pixel being measured. The total air distance between the hot or cold load and the window of the
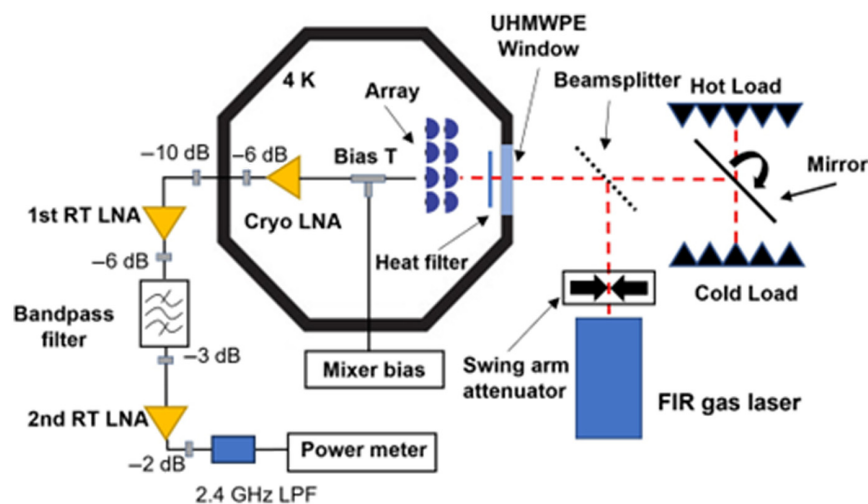
Fig. 2 Experimental setup for measuring double sideband receiver noise temperature ($T_{\mathrm{rec}}^{\mathrm{DSB}}$), receiver conversion loss ($L_{\mathrm{rec}}^{\mathrm{DSB}}$) and optimum LO power ($P_{\mathrm{LO}}$). The hot and cold loads and the beam splitter are in the air. We use the rotating mirror to change between the hot and cold load. The IF NBW was measured using the same setup, but the part including the band pass filter, 2nd RT LNA, 2.4 GHz LPF, and the power meter is replaced with a spectrum analyzer.

cryostat is $\approx$30 cm. In the schematic, we also show an array, which is mounted on the 4 K plate of the cryostat. However, only one pixel could be measured at a time because we could not perform the measurements of all the pixels simultaneously, limited by our setup. The physical temperature of the mixers during the measurements was 4.3 K for B3 and 5.2 to 5.4 K for B1 and B2. The reason for this variation was caused by the need to use an interface plate that in the case of B1 and B2 had a reduced thermal conductance to the cold plate when compared to the one used for B3.

The IF chain consists of a bias-T and a cryogenic SiGe LNA.[48] The latter is connected thermally to the 4 K plate. The room temperature part of the IF chain includes two LNAs, a bandpass filter, a 2.4 GHz low pass filter (LPF), and a microwave power meter. For T_{rec}^{DSB} measurements, the IF was filtered by the bandpass filter with a bandwidth of 100 MHz, centered at 2 GHz. The IF chain had a total gain of 85 dB and a noise temperature of 6.5 K at 2 GHz. For the NBW measurements, we replaced the components from the bandpass filter up to the power meter in Fig. 2 with a spectrum analyzer.

4 Results and Discussion

4.1 Pixel Characterization and Analysis

In Fig. 3, we present, as an example, the characterization of an HEB mixer from the B3 array at 5.25 THz. Figure 3(a) shows three measured current-voltage (IV) curves of the HEB in the unpumped state, when no LO is applied, and two pumping states around the optimum P_{LO}, where the T_{rec}^{DSB} becomes the lowest. The T_{rec}^{DSB} is obtained using the Y-factor technique.[49] In Fig. 3(b), we present an example of a Y-factor measurement for the same pixel. In this case, the lowest T_{rec}^{DSB} is 2110 ± 100 K when the device is biased at a current of 32 μA and a voltage of 1 mV. For this particular bias point, the L_{rec}^{DSB} obtained using a modified version[51] of the U factor technique[52] is 12.7 ± 0.4 B. Applying the modified U factor technique, we do not require the use of a circulator. The details of our methodology and validity are described in Appendix I of this paper. Using the isothermal technique,[53] we estimate the P_{LO} for the same mixer to be between 192 and 199 nW. The optimal operation region in the IV, where we obtain less than 5% degradation of the T_{rec}^{DSB}, covers a voltage range between 0.6 to 1.0 mV and currents between 28 and 40 μA, which is highlighted in Fig. 3(a).

As discussed in the previous section we are interested in T_{mixer}^{DSB} and L_{mixer}^{DSB}. In our case, we define T_{mixer}^{DSB} as the noise temperature after subtracting the noise contributions from all the optics in front of the Si lens and those from the IF chain. For clarity, T_{mixer}^{DSB} in this way includes both the optical loss of the Si lens and power coupling loss due to the impedance mismatching between the antenna and the bolometer. This is different from the intrinsic mixer noise temperature that is determined by the HEB itself and would consider removing any contributions that are not the mixer itself. L_{mixer}^{DSB} is defined as the conversion loss after subtracting the optics in front of
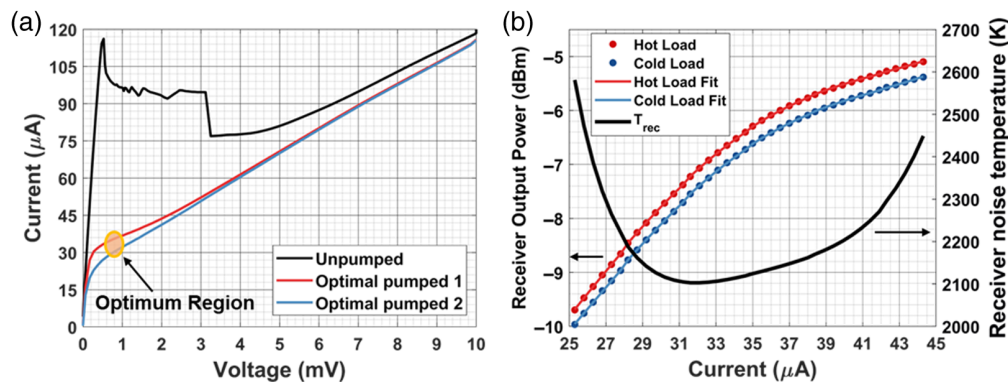
Fig. 3 Characterization of a mixer out of the B3 array at 5.3 THz. (a) Unpumped and optimally pumped current-voltage curves. Highlighted optimum region, where the T_{rec}^{DSB} degrades less than 5% from the lowest value. (b) Examples of measured receiver output powers, responding to both hot and cold loads, are plotted as a function of current at a bias voltage of 1 mV and respective polynomial fit as a function of the HEB bias current, and the resulting T_{rec}^{DSB}.

Table 3 Optical losses including the air, 3-μm thick Mylar beam splitter (BS), window at room temperature, and the heat filter at 4 K in our heterodyne measurement setup.

Array	LO frequency (THz)	Air (dB)	Mylar BS (dB)	Window (dB)	Heat filter (dB)	Total optical losses (dB)
B1	1.39	0.87	0.07	0.43	0.66	2.03
B2	1.63	0.64	0.09	0.38	1.14	2.25
B3	5.25	0.9	0.63	1.47	0.56	3.56

Among them, BS losses are simulated, air loss at 5.3 THz was measured, whereas the air losses at the other two frequencies are simulated. The remaining loss values are measured.

the Si lens. To derive $T_{\text{mixer}}^{\text{DSB}}$ from the measured $T_{\text{rec}}^{\text{DSB}}$ and $L_{\text{rec}}^{\text{DSB}}$, we apply the following formula from Eq. (1)

$$T_{\text{mixer}}^{\text{DSB}} = \frac{T_{\text{rec}}^{\text{DSB}} - T_{\text{Opt}} - T_{\text{IF}} \times L_{\text{rec}}^{\text{DSB}}}{L_{\text{Opt}}}, \qquad (1)$$

where T_{Opt} and L_{Opt} are the noise temperature and losses, respectively, caused by the optics in the optical path between the hot/cold load and the Si lens as shown in Fig. 2, and TIF is the measured noise temperature of the IF chain. It equals 6.5 K and includes the contributions of all the components. The optical losses at different frequencies in our measurements are summarized in Table 3.

Because the B2 and B3 arrays were characterized at different frequencies than those used in GUSTO, we need to convert between them to compare their performance with GUSTO's requirements. Based on Zhang et al.,[13] it can be concluded that, after accounting for optical losses and IF contributions, the mixer's performance closely follows the quantum noise behavior, scaled by a constant factor. The devices used in GUSTO are very similar to those in that study. Therefore, assuming the mixer's conversion loss is relatively constant across nearby frequencies, we can estimate the performance of the mixer arrays at the target GUSTO frequencies from their performance at the experimental frequencies.

For the B2 pixels, we estimate that at 1.9 THz, the mixer noise temperature, $T_{\text{mixer}}^{\text{DSB}}$ be 5% higher than the measured value at 1.63 THz, based on the work in Ref. 13 and our lab's previous experiments. In the case of the B3 pixels, the larger frequency difference requires calibration measurements. To characterize the mixer at 4.7 THz, we used a QCL with a 4.68 THz LO. Due to the high atmospheric absorption at this frequency, we conducted the measurements at both 5.25 and 4.68 THz using a vacuum setup, similar to that described in Ref. 54. Our setup included a 32-mm rotating mirror positioned 170 mm from the HEB, and a cold load with a 35-mm diameter placed 60 mm beyond the mirror. Based on these measurements, we estimate that $T_{\text{mixer}}^{\text{DSB}}$ at 4.7 THz is 7.5% lower than the value measured at 5.25 THz. For the B1 array, the difference in frequency between the LO used for characterization and the LO of B1 is so small that no conversion is required.

To illustrate how we derive a $T_{\text{mixer}}^{\text{DSB}}$ from a measured $T_{\text{rec}}^{\text{DSB}}$, we take the same B3 array pixel used for the measurements in Fig. 3, as an example. We first apply Eq. (1) to the lowest measured $T_{\text{rec}}^{\text{DSB}}$ (2100 K), using Topt = 342 K, $L_{\text{rec}}^{\text{DSB}} = 13.6$ dB and $L_{\text{Opt}} = 3.56$ dB, to derive the $T_{\text{mixer}}^{\text{DSB}}$ at 5.3 THz. Afterward, by applying a reduction factor of 0.925 (corresponding to 7.5%) to the data at 5.3 THz, we derive a $T_{\text{mixer}}^{\text{DSB}}$ at 4.7 THz, which is 665 ± 40 K.

To measure the NBW of an HEB mixer in our arrays, we repeat $T_{\text{rec}}^{\text{DSB}}$ measurements at many intermediate frequencies between 0.5 and 5 GHz. This is done using a spectrum analyzer while biasing the device at a voltage of 1 mV and a current of 32 μA, within the optimal operation region. In Fig. 4, we show one measurement for a B1 pixel at 1.39 THz, where the measured $T_{\text{rec}}^{\text{DSB}}$ is plotted as a function of IF frequency. By fitting a generic exponential equation, $T_{\text{rec}}^{\text{DSB}} = T_0 + a * \exp(\frac{f}{b})$, to the measured data, we find the frequency where the fitted $T_{\text{rec}}^{\text{DSB}}$ increases by 3 dB, which determines the NBW and is 3.5 GHz. We also measured NBW of the same HEB at 5.25 THz and found a value that agrees with the one measured at 1.39 THz.
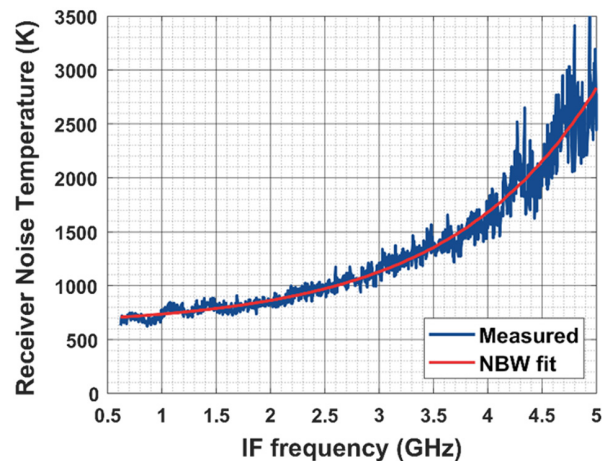
Fig. 4 NBW measurement for a B1 pixel at 1.39 THz. The measured receiver noise temperature as a function of the IF frequency was fitted with a generic exponential equation. From the fitted curve, we estimate an NBW of 3.5 GHz, defined as the frequency at which the receiver noise temperature increases by 3 dB.

Because the NBW is LO frequency independent, two measurements with the same value suggest our experimental results to be reliable and reproducible. The measured NBW is sufficient to fully meet the IF bandwidth requirements for B1 and B2 arrays for GUSTO but is slightly smaller than what is required for B3. We would like to argue that this NBW is expected because it is limited by the NbN film technology used, specifically due to the film thickness of 5 to 6 nm in practice[55,56] and a Si substrate used. The measured NBW here is close to the one previously reported in an NbN HEB produced in our labs from a different film in Ref. 57, which was 4 GHz at 4.7 THz. It also agrees with the NBW results reported for the mixers used in upGREAT, which were 4 GHz for the mixers at 1.9 and 4.7 THz,[18] and those in Ref. 58, which were between 3 and 3.5 GHz. It should be noted that IF bandwidths up to 5 to 6 GHz can be achieved using a different substrate, as mentioned in Ref. 59, which could have benefited the 4.7 THz array in GUSTO.

4.2 HEB Mixer Array Results

The average and standard deviation values for the measured T_{rec}^{DSB}, L_{rec}^{DSB}, and PLO for all the pixels in the three arrays are summarized in Table 4.

We then applied the same methodology described in the previous section to derive the performance for all pixels in the arrays, converting these to the respective operating frequencies in GUSTO. The converted performance data are presented in Fig. 5, which shows the performance for all the pixels in the three arrays at the GUSTO operating frequencies. Here, T_{mixer}^{DSB} are shown in panel (a), L_{mixer}^{DSB} in panel (b), and P_{LO} in panel (c). For P_{LO}, this parameter remains constant as long as the detector is operated at the same bias point and physical temperature. This means the measured P_{LO} value for each array is constant even if operated at different THz frequencies.

Table 4 Measurement summary of the three HEB mixer arrays averaged over the 8 pixels in an array.

Array	Measurement frequency (THz)	T_{rec}^{DSB} (K)	L_{rec}^{DSB} (dB)	P_{LO} (nW)
B1	1.39	700 (19)	7.3 (0.6)	210 (12)
B2	1.63	870 (28)	8.8 (0.7)	190 (10)
B3	5.25	2190 (74)	12.5 (0.7)	240 (15)

It includes the measured received noise temperature (T_{rec}^{DSB}) and receiver conversion loss (L_{rec}^{DSB}) at 2 GHz IF, and optimum LO power at HEB (P_{LO}). In parentheses are the standard deviations within the respective array.

(a)   (b)   (c)
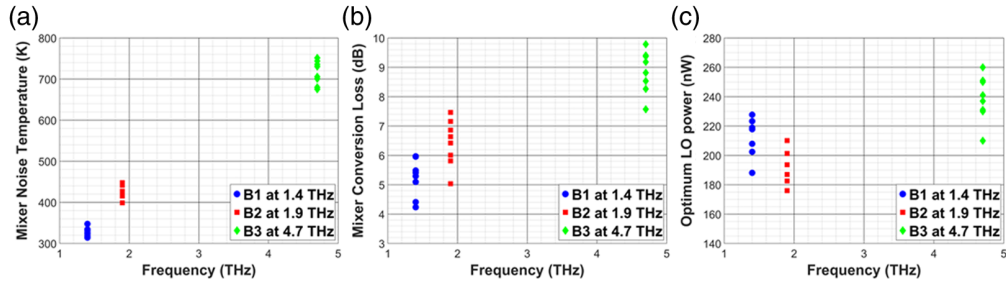
Fig. 5 Mixer noise temperature at 2 GHz IF (a), mixer conversion loss (b), and optimum LO power (c) for the different elements of three HEB mixer arrays characterized at GUSTO's frequencies, 1.46, 1.9, and 4.7 THz.

Table 5 Performance summary of the three HEB mixer arrays averaged over the 8 pixels in an array.

Array	Operating frequency (THz)	$T_{\text{mixer}}^{\text{DSB}}$ (K)	$L_{\text{mixer}}^{\text{DSB}}$ (dB)	$T_{\text{rec,GUSTO}}^{\text{DSB}}$ (K)
B1	1.46	330 (10)	5.2 (0.6)	≈750
B2	1.9	425 (14)	6.4 (0.7)	≈1000
B3	4.7	715 (27)	8.9 (0.7)	≈1650

It includes the measured mixer noise temperature ($T_{\text{mixer}}^{\text{DSB}}$) and mixer conversion loss ($L_{\text{mixer}}^{\text{DSB}}$) at 2 GHz IF, the receiver noise temperature ($T_{\text{rec,GUSTO}}^{\text{DSB}}$), which was estimated when we applied the GUSTO optics and the measured $T_{\text{mixer}}^{\text{DSB}}$ and $L_{\text{mixer}}^{\text{DSB}}$. In parentheses are the standard deviations within the respective array.

To illustrate the array performance, we summarize the average and standard deviation values of $T_{\text{mixer}}^{\text{DSB}}$ and $L_{\text{mixer}}^{\text{DSB}}$ for each array in Table 5, along with the expected performance in the GUSTO receiver.

The average $T_{\text{mixer}}^{\text{DSB}}$ for B1, B2, and B3 arrays are 330, 425, and 715 K, respectively. We demonstrate the arrays' uniformity on $T_{\text{mixer}}^{\text{DSB}}$ in Fig. 5(a), where their standard deviations are within a range of 3% to 4% for the three arrays. An increase of the $T_{\text{mixer}}^{\text{DSB}}$ with the operating frequency is expected. However, the value at 4.7 THz is a factor of 2.1× more than that at 1.46 THz, which is more than was reported in Ref. 13, where the factor for the two same frequencies was about 1.7. This suggests that the increase in $T_{\text{mixer}}^{\text{DSB}}$ is partly due to the contribution of quantum noise and partly due to the additional losses within the mixer, as indicated by the higher $L_{\text{mixer}}^{\text{DSB}}$ at 4.7 THz. The additional losses at 4.7 THz are expected to be caused by the loss in the antenna and the use of the smaller Si lenses (5 mm).[60] For B3 smaller lenses were required to optimize the optical properties of the array to meet the instrument requirements as discussed by Silva et al.[45] The former will be discussed in the next paragraphs. In terms of using the unit of quantum noise (hf/2 k), they are 9.4× hf/2 k at 1.46 THz and 6.2× hf/2 k at 4.7 THz.

For $L_{\text{mixer}}^{\text{DSB}}$, we find that its value increases with the array operating frequency. Such an increase is confirmed even in the intrinsic $L_{\text{mixer}}^{\text{DSB}}$ after removing the optical loss of the lens and coupling loss between the antenna and HEB. This result contradicts the expectation for NbN HEBs because it should be independent of the operating frequency as long as the LO frequency is above the gap frequency of the thin NbN.[13,61] Based on scanning electron microscopy images of some of our devices, we have noticed some artifacts (edge roughness) that are present around the gold spiral antenna arms, which may introduce additional ohmic losses to the THz RF current. This effect would be stronger for a higher frequency and thus could introduce additional RF loss, which was not included in our analysis. The standard deviations for this parameter range between 8% and 11% which is attributed to variations within the same wafer.

The P_{LO} for the B3 array is slightly higher than that for B1 and B2 due to the greater length of the HEBs used in the B3 array. Within a given array the P_{LO} distribution is uniform, with a

standard deviation of around 5–6% consistently for the three arrays. However, for B1 and B3 arrays, we do have one outlier pixel for each array as shown in Fig. 5(c). Nevertheless, even with these two outliers, such P_{LO} uniformity is good enough, allowing to pump all the mixers in the array within their optimum operation regions, where less than 5% degradation of their T_{mixer}^{DSB} is expected. The LO power required at the HEB for the GUSTO arrays is very similar to those used for other instruments. For example, the HIFI HEBs required 200–500 nW;[15] the HEBs at 1.4 THz in STO-2 required ∼220 nW, whereas those at 1.9 THz required a bit lower ∼110 nW.[62] The devices in upGREAT require ∼300 nW.[63]

These arrays have met the performance requirements demanded by the instrument and were used on board of GUSTO during its successful flight. Here, we report only three arrays, however, we have also built and characterized two backup arrays (five arrays in total). One backup array was optimized for 1.6 THz and could have been used to replace either the B1 array or the B2 array, whereas the other one is optimized for 4.7 THz to replace the B3 array if necessary.

We now compare the mixer performance in our arrays with some of the best single-pixel results reported previously in the literature and with the performance of other instruments in the next paragraph. Our average T_{mixer}^{DSB} of 330 K at 2 GHz IF, at 1.46 THz (for B1) is very similar to a T_{mixer}^{DSB} of 300 K at 1.5 GHz IF (measured at 1.3 THz) reported by Zhou et al.,[54,64] which was derived from their T_{rec}^{DSB} (600 K) and the optical losses. Our results are also similar, with a T_{mixer}^{DSB} of ≈300 K at 2 GHz IF and 1.3 THz reported by Krause et al.[59] (see Fig. 7 of the reference). Our average T_{mixer}^{DSB} of 420 K at 2 GHz IF obtained at 1.9 THz (B2) is close to what was reported in our labs, by Zhang et al.,[13] where a T_{mixer}^{DSB} of 380 K at 1.5 GHz IF is derived. In addition, our result for the B2 array is also in line with or even better than the single-pixel T_{rec}^{DSB} of 900 K at 1.5 GHz IF, reported by Kloosterman et al.,[65] and also similar to, or slightly worse than, the T_{rec}^{DSB} of 700 K at 1.6 THz reported by Kroug et al.[66] For the last two references, we are not able to extract exact T_{mixer}^{DSB} due to missing details. Our average T_{mixer}^{DSB} of 700 K at 2 GHz IF, at 4.7 THz (B3) is about 17% higher than the best value reported for a single pixel in our labs, by Kloosterman et al.,[67] for which we estimate a T_{mixer}^{DSB} of 600 K at 2 GHz IF. The difference can be attributed to the loss in the antenna and the use of the smaller Si lenses (5 mm) as discussed previously.

Our arrays, integrated into the GUSTO instrument, have shown a preflight performance as follows: for B1 at 1.4 THz, an averaged GUSTO receiver noise temperature, $T_{rec,GUSTO}^{DSB}$, of 870 K; for B2 at 1.9 THz, an averaged $T_{rec,GUSTO}^{DSB}$ of 1100 K; and for B3 at 4.7 THz, an averaged $T_{rec,GUSTO}^{DSB}$ of 1920 K. All the $T_{rec,GUSTO}^{DSB}$ values above are taken at a physical temperature of 5.1 K for the mixers and an IF frequency of 1 GHz. To compare with our expected receiver noise temperatures in Table 5, the measured values should be converted using a factor of 1.11 which represents the increase in noise temperature from 1 to 2 GHz IF (16% degradation) combined with the lower temperature of the detectors in our measurements (5% improvement). Therefore, the measured $T_{rec,GUSTO}^{DSB}$ are slightly worse than what we expected in Table 5. This can be explained by the fact that in our lab setup for Y-factor measurements, before integration, the entire beam pattern is coupled to the hot/cold load, whereas in GUSTO, there is sidelobe spillover throughout the optics and especially beam vignetting in some optical elements for some of the mixers. These effects contribute to the increase of the noise temperature and hence the differences seen. The GUSTO performance in flight is out of the scope of the present paper and will be addressed in an upcoming publication.

4.3 Scaling the Pixel Count in HEB Mixer Arrays

Although the arrays for GUSTO were designed in a 4 × 2 configuration, the need for both B1 and B2 arrays to be placed side by side on the cold plate of the instrument will demonstrate practically a 4 × 4 mixer array using our array architecture. In this case, care should be taken to ensure the pointing direction of the mixers in one array is parallel to those from another array. The accurate pointing of eight mixers within one array has been demonstrated.[39] Furthermore, in the case of B1 and B2, the final pointing was achieved relative to the same reference, effectively demonstrating the accurate pointing of the pixels between the two arrays.

The above approach allows to extend an array with more pixels, for example, an 8 × 8 pixel array. We argue that we can also build in principle eight 4 × 2 sub-arrays with the right mechanical adaptations, which can be assembled, characterized for their sensitivity and beam pointing

independently, and then mounted on the cold plate of an instrument, such as GUSTO. In terms of the LO, for 1.46 THz, one can build eight sub-arrays of LO based on frequency multiplier chains and combine them to form 64 LO beams. At the higher frequencies, including 1.9 THz, a combination of a QCL with a phase grating could be used to generate 64 LO beams. High-power QCLs have been demonstrated, for example, a 4.7 THz QCL with an output power of 8 mW at 55 K[23] and a 1.8 THz QCL with an output power of 28 mW at 10 K.[68] Based on the GUSTO experience, about 10 mW will be sufficient to pump a 64-pixel array. In addition, a phase grating to generate 81 beams from a single QCL with a high efficiency (94%) has been demonstrated in Ref. 69, which can be applied for generating 64 beams as well. Therefore, we conclude that a large HEB array receiver of 64 pixels is feasible using the current array approach and testing facilities.

5 Conclusions

We have successfully demonstrated three 4 × 2 heterodyne HEB arrays for GUSTO, which were operated at LO frequencies of 1.46, 1.9, and 4.7 THz, respectively. These arrays consist of NbN HEB mixers, where elliptical lenses and spiral antennas are applied to couple the radiation. These arrays represent, to date, the highest pixel count using the quasi-optical scheme at supra-THz frequencies. We have experimentally characterized the arrays over three key parameters, namely the mixer noise temperature (T_{mixer}^{DSB}), mixer conversion loss (L_{mixer}^{DSB}), and optimal LO power (P_{LO}) at the HEB. Our results demonstrate the heterodyne arrays with not only excellent sensitivity, which for example at 4.7 THz is only 6.2× the quantum noise (hf/2 k), but also good uniformity of the performance parameters. The latter is critical for the efficient operation of an array within the instrument. In addition, the measured receiver temperatures at the three frequencies, when arrays are installed in the GUSTO instrument, are also shown. GUSTO launched from Antarctica on the 31st of December 2023 having a successful flight of 57 days, the longest ever recorded by NASA for such mission profile. In addition, our array architecture based on quasi-optical mixers can be scaled up to a large array, e.g., 64 pixels, opening a new avenue toward large heterodyne arrays suitable for future space missions.

6 Appendix A: Conversion Gain Methodology Verification

The typical methodology for measuring the conversion loss requires the use of a circulator between HEB and LNA, as described in Ref. 52. However, our heterodyne measurement setup was designed to measure receiver noise temperatures as well as the IF NBW, necessitating a range of 0.5 to 4 GHz for which no suitable circulators are available. Nonetheless, a modified version of the U-factor[51] can be used to determine the conversion loss if certain conditions are met: the HEB detector can act as a microwave short, and the cryogenic LNA must exhibit very low reflection coefficients (S_{11}).

The first condition is satisfied when the detector is in its superconducting state, causing the HEB to reflect back all power from the LNA. The second condition is also met by our SiGe cryogenic amplifier, which has a relatively low S_{11} within the IF frequencies of interest for the conversion loss measurements. In our case, our LNA has a S_{11} of −20 dB at 2 GHz. This allows us to assume that all the signals from the HEB, either in the operation to respond to the hot load or in the superconducting state, transmit through the LNA. With these conditions validated, we can apply the U-factor equation, but with $T_{REF} = T_{IF} = 6.5$ K, instead of the temperature of the 50 Ω resistor in a circulator, typically 4.2 K. We apply this modified U-factor technique in the present paper.

To validate this approach experimentally, we characterized an HEB mixer around 2 GHz., similar to those used in the GUSTO arrays, both with and without a circulator between the HEB mixer and the SiGe LNA. Without the circulator, we applied the modified U-factor technique as described previously, whereas with the circulator, we used the standard U-factor expression. Measurements showed an ∼1.1 dB increase in conversion loss when using the circulator. Given the circulator's insertion loss of 0.7 dB (at room temperature), the actual difference between the two methods is ∼0.4 dB. This small difference in conversion loss values indicates that our approach is sufficiently accurate. As the devices used in our arrays are very similar,

we consider the observed difference to be the expected error margin in our conversion loss data, i.e., ±0.4 dB. This small error gives only a 1% uncertainty of derived mixer noise temperatures in our case.

Disclosures

The authors declare there are no financial interests, commercial affiliations, or other potential conflicts of interest that have influenced the objectivity of this research or the writing of this paper.

Code and Data Availability

The data that support the findings of this article can be made available upon request to the corresponding authors.

Acknowledgments

References

1. C. K. Walker, "THz coherent detection systems," in *Terahertz Astronomy*, 1st ed., pp. 159–227, Taylor & Francis, New York, NY, USA (2016).
2. C. Pabst et al., "Disruption of the Orion molecular core 1 by wind from the massive star θ 1 Orionis C," *Nature* **565**(7741), 618–621 (2019).
3. Y. M. Seo et al., "Probing ISM structure in Trumpler 14 and Carina I using the stratospheric terahertz observatory 2," *Astrophys. J.* **878**, 120 (2019).
4. K. Tadaki et al., "The gravitationally unstable gas disk of a starburst galaxy 12 billion years ago," *Nature* **560**, 613–616 (2018).
5. R. Güsten et al., "Astrophysical detection of the helium hydride ion HeH+," *Nature* **568**, 357–359 (2019).
6. H. Linz et al., "Bringing high spatial resolution to the far-infrared," *Exp. Astron.* **51**, 661–697 (2021).
7. P. L. Richards et al., "Quasiparticle heterodyne mixing in SIS tunnel junctions," *Appl. Phys. Lett.* **34**(5), 345–347 (1979).
8. J. R. Tucker and M. J. Feldman, "Quantum detection at millimeter wavelengths," *Rev. Mod. Phys.* **57**, 1055–1113 (1985).
9. E. E. Gershenzon et al., "Millimeter and submillimeter range mixer based on electron heating of super conducting films in the resistive state," *Superconductivity* **3**(10), 1582–1597 (1990).
10. T. M. Klapwijk and A. V. Semenov, "Engineering physics of superconducting hot-electron bolometer mixers," *IEEE Trans. Terahertz Sci. Technol.* **7**, 627–648 (2017).
11. D. Farrah et al, "Review: far-infrared instrumentation and technological development for the next decade," *J. Astron. Telesc. Instrum. Syst.* **5**(2), 020901 (2019).
12. A. Wootten and A. R. Thompson, "The Atacama large millimeter/submillimeter array," *Proc. IEEE* **97**(8), 1463–1471 (2009).
13. W. Zhang et al., "Quantum noise in a terahertz hot electron bolometer mixer," *Appl. Phys. Lett.* **96**, 111113 (2010).
14. M. Hajenius et al., "Full characterization and analysis of a terahertz heterodyne receiver based on a NbN hot electron bolometer," *J. Appl. Phys.* **100**, 074507 (2006).
15. S. Cherednichenko et al., "Hot-electron bolometer terahertz mixers for the Herschel Space Observatory," *Rev. Sci. Instrum.* **79**, 034501 (2008).
16. T. de Graauw et al., "The Herschel-Heterodyne instrument for the far-infrared (HIFI)," *Astron. Astrophys.* **518**(L6), 1–7 (2010).
17. C. Walker et al., "The Stratospheric THz Observatory (STO)," *Proc. SPIE* **7733**, 77330N (2010).
18. C. Risacher et al., "The upGREAT dual frequency heterodyne arrays for SOFIA," *J. Astron. Instrum.* **7**(4), 1840014 (2018).
19. J. V. Siles et al., "Development of high-power multi-pixel LO sources at 1.47 THz and 1.9 THz for astrophysics: present and future," in *Proc. 26th Int. Symp. Space Terahertz Technol.*, Vol. 40, p. T1–3 (2015).

20. I. Mehdi et al., "THz diode technology: status, prospects, and applications," *Proc. IEEE* **105**(6), 990–1007 (2017).
21. B. S. Williams, "Terahertz quantum-cascade lasers," *Nat. Photonics* **1**, 517–525 (2007).
22. M. S. Vitiello et al., "Quantum cascade lasers: 20 years of challenges," *Opt. Express* **23**(4), 5167–5182 (2015).
23. A. Khalatpour et al., "A tunable unidirectional source for GUSTO's local oscillator at 4.74 THz," *IEEE Trans. Terahertz Sci. Technol.* **12**(2), 144–150 (2021).
24. B. A. Curwen, J. L. Reno, and B. S. Williams, "Broadband continuous single-mode tuning of a short-cavity quantum-cascade VESCEL," *Nat. Photonics* **13**, 855–859 (2019).
25. C. Mirzaei et al., "Enhanced sensitivity of THz NbN hot electron bolometer mixers," arXiv:2311.02613 (2023).
26. I. A. Murphy, R. Padman, and R. E. Hills, "An experimental submillimeter heterodyne array receiver," *Int. J. Infrared Millim. Waves* **9**(4), 325–350 (1988).
27. U. U. Graf et al., "Terahertz heterodyne array receivers for astronomy," *J. Infrared Millim. Terahertz Waves* **36**, 896–921 (2015).
28. P. F. Goldsmith, "Sub-millimeter heterodyne focal-plane arrays for high-resolution astronomical spectroscopy," *URSI Radio Sci. Bull.* **2017**, 53–73 (2017).
29. C. Walker et al., "Gal/Xgal U/LDB spectroscopic/stratospheric THz observatory: GUSTO," *Proc. SPIE* **12190**, 121900E (2022).
30. I. R. G. Silva et al., "4 × 2 HEB receiver at 4.7 THz for GUSTO," *Proc. SPIE* **10708**, 107080Z (2018).
31. J. Siles et al., "ASTHROS – astrophysics stratospheric telescope for high-spectral resolution observations at submillimeter-waves: mission overview and development status," in *Proc. 31st ISSTT*, Vol. 5 (2020).
32. C. K. Walker et al., "Orbiting astronomical satellite for investigating stellar systems (OASIS): following the water trail from the interstellar medium to oceans," *Proc. SPIE* **11820**, 1182000 (2021).
33. I. C. Wiedner et al., "A proposed heterodyne receiver for the origins space telescope," *IEEE Trans. Terahertz Sci. Technol.* **8**(6), 558–571 (2018).
34. D. Rigopoulou et al., "The far-infrared spectroscopic surveyor (FIRSS)," *Exp. Astron.* **51**, 699 (2021).
35. J. Hesler et al., "Development and testing of the 1.46 THz and 1.9 THz GUSTO flight-model local oscillator arrays," in *Proc. 31st ISSTT*, Vol. 36 (2020).
36. A. Khalatpour, J. L. Reno, and Q. Hu, "Phase-locked photonic wire lasers by π coupling," *Nat. Photonics* **13**, 47–53 (2019).
37. H. Richter et al., "4.7-THz local oscillator for the GREAT heterodyne spectrometer on SOFIA," *IEEE Trans. Terahertz Sci. Technol.* **5**(4), 539–545 (2015).
38. B. Mirzaei et al., "4.7 THz asymmetric beam multiplexer for GUSTO," *Opt. Express* **29**(15), 24434–24445 (2021).
39. J. R. G. Silva et al., "High accuracy pointing for quasi-optical THz mixer arrays," *IEEE Trans. Terahertz Sci. Technol.* **12**(1), 53–62 (2022).
40. A. Gatesman, R. Gilesm, and J. Waldman, "High-precision reflectometer for submillimeter wavelengths," *J. Opt. Soc. Amer. B* **12**(2), 212–219 (1995).
41. W. Zhang et al., "Noise temperature and beam pattern of an NbN hot electron bolometer mixer at 5.25 THz," *J. Appl. Phys* **108**, 093102 (2010).
42. A. D. Semenov et al., "Terahertz performance of integrated lens antennas with a hot-electron bolometer," *IEEE Trans. Microw. Theory Tech.* **55**(2), 239–247 (2007).
43. W. Zhang et al., "Twin-slot antenna coupled NbN hot electron bolometer mixer at 2.5 THz," *IEEE Trans. Terahertz Sci. Technol.* **1**(2), 378–382 (2011).
44. B. D. Jackson, "NbTiN-based THz SIS mixers for the Herschel Space Observatory," PhD dissertation, Faculty of App. Sci., TU Delft, NL (2005).
45. J. R. G. Silva et al., "Beam waist properties of spiral antenna coupled HEB mixers at Supra-THz frequencies," *IEEE Trans. Terahertz Sci. Technol.* **13**(2), 167–177 (2023).
46. A. Gatesman et al., "An anti-reflection coating for silicon optics at terahertz frequencies," *IEEE Microw. Guided Wave Lett.* **10**(7), 264–266 (2000).
47. D. J. Hayton et al., "Stabilized hot electron bolometer heterodyne receiver at 2.5 THz," *Appl. Phys. Lett.* **100**(8), 081102 (2012).
48. S. Weinreb et al., "Matched wideband low-noise amplifiers for radio astronomy," *Rev. Sci. Instrum.* **80**, 044702 (2009).
49. P. Khosropanah et al., "Low noise NbN hot electron bolometer mixer at 4.3 THz," *Appl. Phys. Lett.* **91**, 221111 (2007).
50. I. Hajenius et al., "Full characterization and analysis of a terahertz heterodyne receiver based on a NbN hot electron bolometer," *J. Appl. Phys.* **100**, 074507 (2006).
51. E. Novoselov et al., "Effect of the critical and operational temperatures on the sensitivity of MgB HEB mixers," *IEEE Trans. Terahertz Sci. Technol.* **6**(2), 238–244 (2016).

52. S. Cherednichenko et al., "1.6 THz heterodyne receiver for the far infrared space telescope," *Phys. C: Supercond. Appl.* **372**, 427–431 (2002).

53. H. Ekström et al., "Conversion gain and noise of niobium superconducting hot-electron-mixers," *IEEE Trans. Microw. Theory Tech.* **43**(4), 938–947 (1995).

54. R. Lefèvre et al., "Terahertz NbN hot electron bolometer fabrication process with a reduced number of steps," in *Proc. of the 23rd ISSTT*, Vol. 127 (2012).

55. J. R. Gao et al., "Monocrystalline NbN nanofilms on a 3*C*-SiC/Si substrate," *Appl. Phys. Lett.* **91**, 062504 (2007).

56. J. W. Kooi et al., "IF impedance and mixer gain of NbN hot electron bolometers," *J. Appl. Phys.* **101**(4), 044511 (2007).

57. D. J. Hayton et al., "A 4.7 THz heterodyne receiver for a balloon borne telescope," *Proc. SPIE* **9153**, 91531R (2014).

58. W. Zhang et al., "Temperature dependence of the receiver noise temperature and IF bandwidth of superconducting hot electron bolometer mixers," *Supercond. Sci. Technol.* **27**, 085013 (2014).

59. S. Krause et al., "Noise and IF gain bandwidth of a balanced waveguide NbN/GaN hot electron bolometer mixer operating at 1.3 THz," *IEEE Trans. Terahertz Sci. Technol.* **8**(3), 365–371 (2018).

60. J. R. G. Silva et al., "Preliminary design study of a 4 × 2 HEB array at 4.7 THz for GUSTO," in *Proc. 29th ISSTT*, pp. 82–86 (2018).

61. E. L. Kollberg et al., "Impedance of hot-electron bolometer mixers at terahertz frequencies," *IEEE Trans. Terahertz Sci. Technol.* **1**(2), 383–389 (2011).

62. J. V. Siles et al., "An ultra-compact 16-pixel local oscillator at 1.9 THz," in *Proc. 41st Int. Conf. Infrared, Millim., and Terahertz Waves* (2016).

63. A. Young et al., "Stratospheric terahertz observatory 2016, sub-orbital flight from McMurdo, Antarctica," in *Proc. ISSTT*, Vol. 4 (2017).

64. K. M. Zhou et al., "1.4 THz quasi-optical NbN superconducting HEB mixer developed for the DATE5 Telescope," *IEEE Trans. Appl. Supercond.* **25**(3), 1–5 (2014).

65. J. L. Kloosterman et al., "4-pixel heterodyne receiver at 1.9 THz using a CMOS spectrometer," in *Proc. 28th ISSTT*, Vol. 74 (2017).

66. I. Kroug et al., "NbN hot electron bolometric mixers for terahertz receivers," *IEEE Trans. Appl. Supercond.* **11**(1), 962–965 (2001).

67. J. L. Kloosterman et al., "Hot electron bolometer heterodyne receiver with a 4.7-THz quantum cascade laser as a local oscillator," *Appl. Phys. Lett.* **102**, 011123 (2013).

68. S. Kumar et al., "A 1.8-THz quantum cascade laser operating significantly above the temperature of $\hbar\omega/k_B$," *Nat. Phys.* **7**, 166–171 (2011).

69. Y. Gan et al., "81 supra-THz beams generated by a Fourier grating and a quantum cascade laser," *Opt. Express* **27**, 34192–34203 (2019).

70. J. R. G. Silva et al., "4 × 2 Hot electron bolometer mixer arrays for detection at 1.4, 1.9 and 4.7 THz for a balloon borne terahertz observatory," *Proc. SPIE* **13102**, 1310239 (2024).

Biographies of the authors are not available.